Electrical Capacitance Tomography with a Variable Topology

Stephan Mühlbacher-Karrer
Institute of Smart System Technologies,
Sensors and Actuators
Alpen Adria Universität, Klagenfurt
9020 Klagenfurt, Austria
stephan.muehlbacher-karrer@aau.at

Hubert Zangl
Institute of Smart System Technologies,
Sensors and Actuators
Alpen Adria Universität, Klagenfurt
9020 Klagenfurt, Austria
hubert.zangl@aau.at

Abstract— **In this paper we present a novel approach for Electrical Capacitance Tomography (ECT) with a variable electrode topology of the sensor front end. The topology of the ECT can be continuously varied while the reconstruction takes place. The unique combination of light weight signal processing chain with a variable dual plate planar sensor front end meets the usability and performance requirements of robotic and mobile applications. The experimental results show the feasibility of this approach achieving reconstruction results with low artefacts even with a low number of electrodes not only in the vicinity of the electrodes but also in the center of the Region of Interest (ROI). Moreover, this sensor topology can be miniaturized which eases the integration, e.g., on a robot's end effector.**

Keywords- Electrical capacitance tomography; capacitive sensing; variable topology; Box-Cox transformation

I. INTRODUCTION

In the past ECT was studied intensively for industrial applications such as flow measurement for oil and gas [1], [2]. In this paper we present a novel approach to use ECT with a variable electrode topology as shown in Figure 1. In our setup the electrode topology can change over time. The distance between both planar surfaces of the sensor front end can be varied in a range of $d_y = 0 - 0.095$ m in the same way as, e.g., a two finger parallel gripper opens and closes its fingers while grasping an object. This also implies that the change of the topology during a single measurement cycle is small enough in comparison to the change of the measurement signals. Therefore, the measurement speed of the hardware must be sufficiently high, usually greater than 1 kHz, to obtain a complete measurement matrix and to compute the reconstruction image. In addition, this approach can handle uncertainties of the sensor front end's position, increasing the robustness of the reconstruction process. This unique combination of ECT with a variable electrode topology approach, measurement hardware, supporting a measurement rate up to 6.25 kHz, and reconstruction algorithm with real time capability meets the performance and usability requirements of robotic applications.

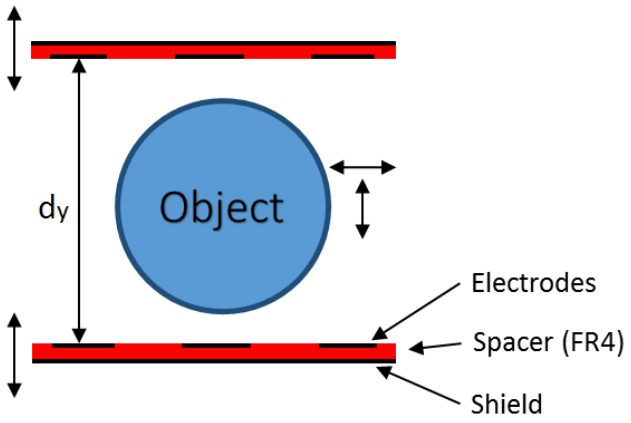

Figure 1. Sketch (2D cross section) of the sensor front end topology comprimising two moveable planes with three electrodes on each.

II. RELATED WORK

ECT is an inverse problem which uses capacitance measurements to determine the permittivity distribution of a certain domain also referred to as ROI. In the classical setup, the ROI is usually a cross section of a pipe where all the electrodes are located at the circumference of the pipe [3], [4] and [5]. An excitation signal is applied in sequence on the sensor electrode array and the inter electrode capacitances between the excitation electrode and the remaining electrodes are measured. Using this information, and solving the inverse problem, an image of the permittivity distribution of the ROI can be obtained. In ECT the environment including the topology of the electrodes is well known in advance. It is a soft field problem due to the bending of the electric field lines, reducing the resolution of the reconstruction images, in comparison to hard-field tomography systems like x-ray. The main advantage of ECT is the comparatively moderate hardware complexity together with little space requirement compared to other tomography systems such as γ-ray, and it is a non-invasive method [6]. Recently the application range of ECT systems was extended by the increasing demand on planar sensor geometries. This is done by changing the classical electrode topology by enrolling it to a planar surface. In previous work [7] we have shown good results for static

planar geometries with heavy signal processing reconstruction algorithms. However, neither measurement speed nor the reconstruction speed of the applied reconstruction algorithm were usable in terms of real time capability to be able to apply ECT in the field of robotic applications.

In [8] it was shown that the ECT approach using single planar sensing surfaces can be used for proximity sensing giving the advantage not only to detect an object but also estimate the position. In addition, also subregions of the reconstruction image can be selected.

Recently in [9] the authors reported a two plate ECT sensor where different number of electrodes and sensor plate distances are evaluated with two linear reconstruction algorithm, Linear Backprojection (LBP) and Landweber iterations. In [10] a dual plane configuration is shown for 3D reconstruction with a fixed distance between two planar sensor planes.

In the last two decades a bunch of reconstruction algorithms was developed, each coming with individual properties in terms of computational effort, image quality and field of application. The simplest class of algorithm is the LBP [11] where so called sensitivity information and linearization is used for the reconstruction. The advantage of the LBP is the high speed of this algorithm. In comparison, Nonlinear Iterative (NI) [12] methods come with the advantage of high quality images, however, the computational effort increases tremendously. In Kalman Filters (KF) [13] a process model is used and the state of the model is estimated using the information of the obtained measurements. Markov Chain Monte Carlo (MCMC) [14] come with a very high computational complexity, making this group of algorithms less attractive for real time applications.

Optimal Approximation (OA) [15] was first suggested in 2007 where the computational complexity is kept at the same level as LBP but by incorporating the prior knowledge, the quality of the reconstruction images can be improved significantly. The achieved tradeoff between reconstruction speed and image quality of Optimal First Order Approximation (OFOA) presented in [8] makes this algorithm an excellent choice to combine a variable sensor topology and mobile applications with limited hardware resources. In addition, in [16] it was shown that artefacts which may occur in regions with low permittivity can be reduced by applying non-linear transformation, e.g., Box Cox where a review of investigations can be found in [17].

III. SYSTEM DESCRIPTION

A. Sensor Front End

The sensor front end consists of two planar surfaces (Printed Circuit Boards (PCBs)) with three electrodes on each. In [7] we obtained feasible reconstruction results with the used electrode topology. Consequently, we decided to use an electrode topology with six electrodes for this work. The electrodes are 12 mm x 152 mm x 0.035 mm (width x depth x height) in size and the distance between the adjacent electrodes is 15 mm. A shield layer (connected to ground in this setup) on the backside of the PCB is used to be insensitive to disturbances on the rear side of the sensor. The space between adjacent electrodes is connected to the shield layer of the PCB. Both sensor planes can be continuously moved on the translation stage to vary the distance between the electrodes as shown in the measurement setup in Figure 4. Objects can move randomly around between both sensor planes. The setup is configured in the differential measurement mode where the capacitance between two electrodes is determined. The properties including benefits and drawbacks of the measurement mode are discussed in [18]. Applying the excitation signal in sequence on each electrode while measuring the displacement current on the remaining receiver electrodes in each sequence step. Consequently, the maximum number of independent measurements N can be calculated $N = \frac{n(n-1)}{2} = 15$, where n is the number of electrodes.

B. Fast Bayesian Reconstruction and Artefact Reduction

In this section we provide a summary of [16] where we first introduced the combination of OA and artefact reduction in one algorithm. The aim of this reconstruction approach is to find a function f_i minimizing the mean square error between the reconstructed permittivity distribution $\hat{\varepsilon}$ and the real permittivity distribution ε in the ROI. Further on we are seeking for an optimal reconstruction function $f_{i,opt}$ out of a set of ϕ reconstruction functions given by

$$f_{i,opt} = arg \min_{f_i \epsilon \phi} E\{(\hat{\varepsilon} - \varepsilon)^2\} \quad (1)$$

An optimal estimator to minimize the mean square error to solve (1) is the expected value of ε conditioned on the measurements y and is given by

$$\hat{\varepsilon}_{MMSE} = E\{\varepsilon|y\} \approx Wy + B \quad (2)$$

Where the expected value $E\{\}$ is approximated by an affine transformation of the measurement vector leading to the Linear Minimum Mean Square Error (LMMSE) approach. This approach boosts the reconstruction speed to meet the speed requirement of the reconstruction algorithm. The optimal solution for (2) is found with

$$W = C_{\varepsilon Y} C_{YY}^{-1} \quad (3)$$

and

$$B = \bar{\varepsilon} - W\bar{y} \quad (4)$$

where the auto-covariance matrix of the measurements is expressed by C_{YY}^{-1} and the cross-covariance matrix between the measurements and the permittivities is expressed by $C_{\varepsilon Y}$. The expected permittivity according to the prior probability is $\bar{\varepsilon}$ and the expected value of the measurements is $\bar{y}$ [8], [16].

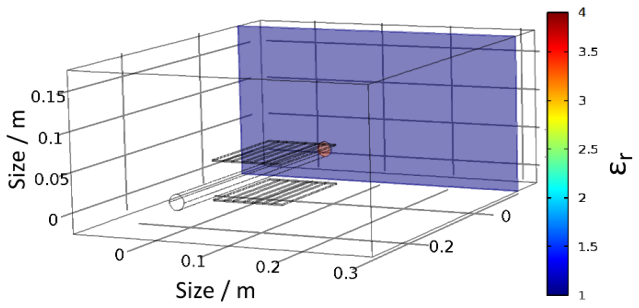

Figure 2. 3D model of the finite element simulation to solve the forward problem. The topology is according to the setup given in Figure 1.

Due to the strong nonlinearity in regions with low permittivity values, OSOA may cause artefacts in this regions. To avoid this error we apply the non-linear Box-Cox transformation to the permittivity values sampled from the prior distribution given by

$$\varepsilon_i^{(\lambda)} = \begin{cases} \frac{\varepsilon_i^{\lambda}-1}{\lambda} & \lambda \neq 0 \\ \log \varepsilon_i & \lambda = 0 \end{cases} \tag{5}$$

The transformation parameter is set to $\lambda = 0.4$ in our setup where a grid search approach is used, minimizing

$$\lambda = arg \min_{\tilde{\lambda} \in \Re} \left(E\{WY + B - \varepsilon^{\tilde{\lambda}}\} \right) \tag{6}$$

to find the optimal value for λ. For each element of ε given in (5) the Box-Cox transformation is applied [16], represented by $\varepsilon^{\tilde{\lambda}}$.

C. Simulation Framework

The choice of the prior distribution of ε in Eq. (1) is crucial for the reconstruction process. Consequently, the prior distribution must be defined in a reasonable way for each electrode topology $d_y = 0 - 0.095$ m used in the setup. To realize the samples of the prior distribution, the forward problem is solved offline for each assumed material distribution and electrode topology. This comes with the advantage that for each offline computation only a minor online computational effort is necessary.

To solve the forward problem, a 3D simulation model is setup using the solver COMSOL. We implemented a MATLAB framework including an Application Programming Interface (API) to handle variable electrode topologies and different objects to obtain the necessary simulation data. This simulation framework provides the flexibility to easily swap the prior distribution for the reconstruction process. The 3D simulation model is shown in Figure 2. The simulation is done in 3D however, the reconstruction images are provided as 2D cross sections of the ROI.

The forward problem is solved twice to avoid errors introduced by remeshing the 3D model while the objects are repositioned in the ROI. First, the problem is solved for $\varepsilon_r = 1$ and the second time the problem is solved using the

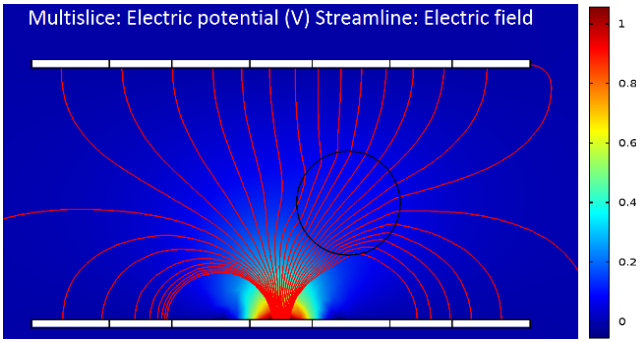

Figure 3. Topview of the 3D finite element simulation of the electric field (red lines) and potential (colorbar) for a sample of the prior distribution. The electric field is distorted by the object depening on its position. The topology is according to the setup given in Figure 1.

desired value ε_r of the object, e.g., PVC $\varepsilon_r = 3.4$. In Figure 3 the electric potential and electric field lines are shown while electrode two is excited and an object is present in the ROI. It should be noted that the electric field lines expand to the distant ground of the 3D model not visible in the image section. The simulations are carried out in steps of $\Delta d_y = 5$ mm. This step size is sufficient as our reconstruction algorithm is capable to handle these uncertainties of the position of the sensor front end.

IV. Experimental Setup

The test bench to carry out all experiments is shown in Figure 4. The translation stage is used for both to move the objects and the sensor planes precisely. The maximum distance between the sensor front ends is $d_y = 0.095$ m. The objects are moved in an area of $x = 0 - 0.1$ m and

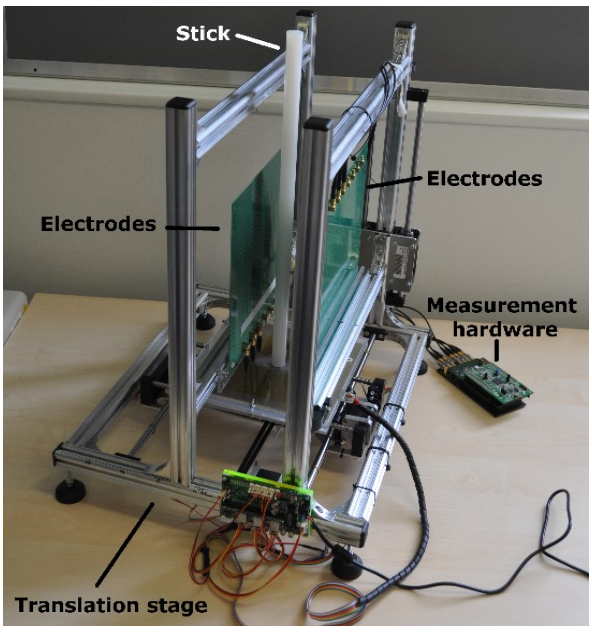

Figure 4. The ECT measurement setup for variable electrode topology comprising the measurement hardware using six input channels, the translation stage to move an object (stick made of erthalon) and the plane sensor front ends consisting of three electrodes and a shield on the back side.

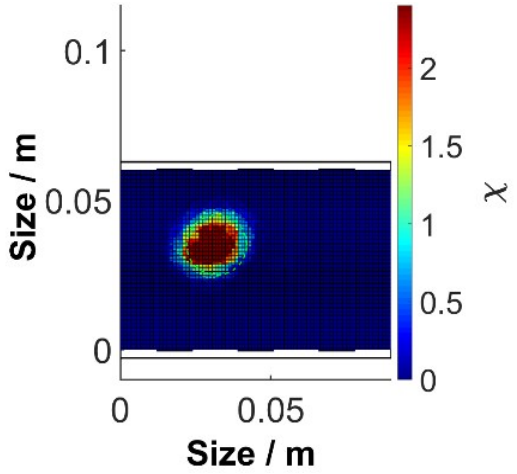

Figure 5. Reconstruction image with a distance of $d_y = 0.06\,m$ between the planar sensor front ends. The three electrodes and shield layer are depicted by black lines at the top and bottom of the ROI. The area with the highest susceptibility matches the true position (dashed green line) of the object very well. In addition, no artefacts are visible in the ROI.

$y = 0 - d_y$ (ROI). The sample object is made of Erthalon ($\varepsilon_r = 3.9$) with a diameter of $d_s = 20$ mm for all experiments. The experiments are carried out in the lab at room temperature.

The measurement hardware is connected via coaxial cables to the electrodes of the two sensor planes. It is configured in the differential measurement mode where a sine wave excitation signal with a frequency of $f_{ex} = 1$ MHz is used for all experiments carried out. The measurement circuit is implemented as low impedance measuring the displacement current on the receiver side using I/Q demodulation [19].

To compensate offset errors, the results of our 3D simulation with the obtained measurement values of the measurement hardware, an offset calibration is applied for each element of the measurement vector $\boldsymbol{y}$ given as

$$y[n] = y_{raw}[n] - y_{air}[n] \tag{3}$$

where measurement values while no object is located in front of both sensor planes is expressed by y_{air} and raw measurement values are expressed by y_{raw}. The calibration measurement to obtain y_{air} is done once in advance.

V. Experimental Results

In this Section the experimental results are presented. The images show the electric susceptibility χ which is related to the permittivity in the following form $\chi = \varepsilon_r - 1$. The reconstruction results show snapshots for different electrode positions $d_y = 0.06$ m, $d_y = 0.08$ m and $d_y = 0.095$ m and an object randomly positioned in the ROI.

The reconstruction result in Figure 5 shows that the object can be reconstructed at its true position. In addition, the objects can be reconstructed in the complete ROI not only in the vicinity of the electrodes in comparison to the single planar sensor front end in [8].

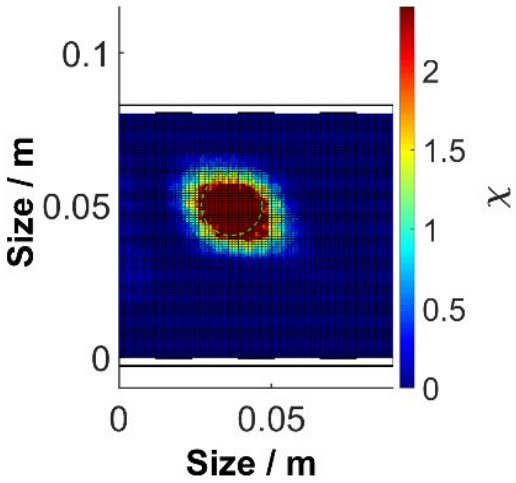

Figure 6. Reconstruction image with a distance of $d_y = 0.08\,m$ between the planar sensor front ends. The three electrodes and shield layer are depicted by black lines at the top and bottom of the ROI. The area with the highest susceptibility matches the true position (dashed green line) of the object very well. However, the true susceptibility value does not exactly match the real susceptibility of the object.

Even with increasing distance between electrodes as shown in Figure 6 objects close to the center of the ROI can be reconstructed very well. Also the shape and position accuracy matches the true object.

In Figure 7 the maximum range of the electrode distance is shown for this system. In this case, the object can be reconstructed very well in the vicinity of the electrodes. Furthermore, for the example shown in Figure 7, the use of the Box Cox transformation reduces the mean square error in regions, where no object is present by about 64 %, thus, it tremendously improves the accuracy of the reconstruction image. However, the reconstruction image quality decreases to the center of the ROI due to the increasing distance between

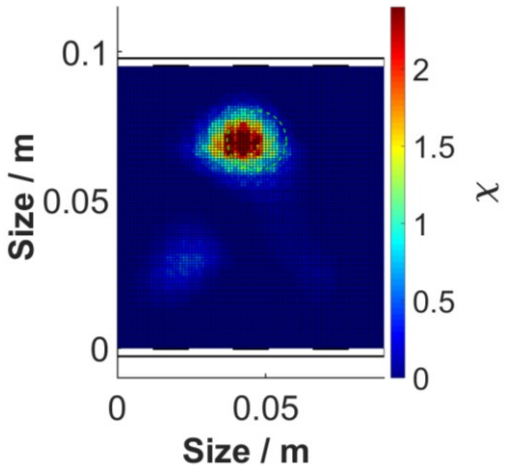

Figure 7. Reconstruction image with a distance of $d_y = 0.95$ m between the planar sensor front ends. The three electrodes and shield layer are depicted by black lines at the top and bottom of the ROI. The area with the highest susceptibility and the true position (dashed green line) of the object have a close match even if some artefacts occur to the bottom left side of the image.

the sensor electrodes and the distance to the object in the ROI. For increasing distances $d_y > 0.095$ m the Signal to Noise Ratio (SNR) is too low to obtain feasible reconstruction results for the entire ROI. However, the reconstruction in the vicinity of the electrodes is still possible. Due to the open sensing area to the left and right side of the ROI no feasible reconstruction results can be obtained in this area.

The reconstruction results show that the suggested approach is feasible to be used on robotic application such as a robot's end-effector for parallel grasping. The sensing range strongly depends on the size and topology of the electrodes and can be easily tailored, e.g., to a robot's end-effector and the needs of the application. A reduction of artefacts in the reconstruction images as achieved by using the Box Cox transformation is particularly useful for object detection, e.g., in collision avoidance systems, as the rate of false alarms can be significantly reduced.

VI. Conclusion

In this paper we extended the ECT approach to use with a variable electrode topology. The electrode topology can vary during the measurement and reconstruction process. With the proposed electrode topology sensing ranges up to 0.095 m can be covered even with a limited number of six electrodes. The experimental setup and results show the feasibility of this approach which can be further adopted to the needs of a certain application.

References

[1] I. Ismail, J. Gamio, S. A. Bukhari, and W. Yang, "Tomography for multi-phase flow measurement in the oil industry," Flow Measurement and Instrumentation, vol. 16, no. 2, pp. 145–155, 2005.

[2] C. Xie, S. Huang, B. Hoyle, R. Thorn, C. Lenn, D. Snowden, and M. Beck, "Electrical capacitance tomography for flow imaging: system model for development of image reconstruction algorithms and design of primary sensors," Circuits, Devices and Systems, IEE Proceedings G, vol. 139, no. 1, pp. 89–98, Feb 1992.

[3] W. Yang and L. Peng, "Image reconstruction algorithms for electrical capacitance tomography," Meas. Sci. Technol., vol. 14, no. 1, pp. R1-R13, January 2003.

[4] O. Isaksen, "A review of reconstruction techniques for capacitance tomography," Measurement Science and Technology, vol. 7, pp. 325–337, 1996.

[5] A. Plaskowski, M. Beck, R. Thorn, and T. Dyakowski, Imaging Industrial Flows: Applications of Electrical Process Tomography. Taylor & Francis, 1995.

[6] M. Neumayer, H. Zangl, D. Watzenig, and A. Fuchs, "Current reconstruction algorithms in electrical capacitance tomography," in New Developments and Applications in Sensing Technology, ser. Lecture Notes in Electrical Engineering. Springer Berlin Heidelberg, 2011, vol. 83, pp. 65–106.

[7] T. Schlegl, M. Neumayer, S. Mühlbacher-Karrer, and H. Zangl, "A pretouch sensing system for a robot grasper using magnetic and capacitive sensors," Instrumentation and Measurement, IEEE Transactions on, vol. 62, no. 5, pp. 1299–1307, May 2013.

[8] S. Mühlbacher-Karrer and H. Zangl, "Object detection based on electrical capacitance tomography," in IEEE Sensors Applications Symposium, 2015.

[9] Z. Ren and W. Yang, "A miniature two-plate electrical capacitance tomography sensor," Sensors Journal, IEEE, vol. 15, no. 5, pp. 3037–3049, 2015.

[10] H.-Y. Wei, C.-H. Qiu, and M. Soleimani, "Evaluation of planar 3d electrical capacitance tomography: from single-plane to dual-plane configuration," Measurement Science and Technology, vol. 26, no. 6, p. 065401, 2015.

[11] C. Xie, S. Huang, B. Hoyle, R. Thorn, C. Lenn, D. Snowden, and M. Beck, "Electrical capacitance tomography for flow imaging: system model for development of image reconstruction algorithms and design of primary sensors," Circuits, Devices and Systems, IEE Proceedings G, vol. 139, no. 1, pp. 89–98, Feb 1992.

[12] M. Soleimani and W. Lionheart, "Nonlinear image reconstruction for electrical capacitance tomography using experimental data," Measurement Science and Technology, vol. 16, pp. 1987–1996, October 2005.

[13] H.-C. Kim, K. Kim, J. Park, and H. Lee, "Electrical impedance tomography reconstruction algorithm using extended kalman filter," in Industrial Electronics, 2001. Proceedings. ISIE 2001. IEEE International Symposium on, vol. 3, 2001, pp. 1677–1681 vol. 3.

[14] J. P. Kaipio and E. Somersalo, Statistical and Computational Inverse Problems. Applied Mathematical Sciences, Springer Verlag New York, Inc., 2004

[15] H. Zangl, D. Watzenig, G. Steiner, A. Fuchs, and H. Wegleiter, "Noniterative reconstruction for electrical tomography using optimal first and second order approximations," in Proceedings of the 5th World Congress on Industrial Process Tomography, Bergen, Norway, September 3-6, 2007, pp. 216–223.

[16] H. Zangl and S. Mühlbacher-Karrer, "Artefact reduction in fast Bayesian inversion in electrical tomography," COMPEL-The international journal for computation and mathematics in electrical and electronic engineering (in press).

[17] R. Sakia, "The box-cox transformation technique: a review," The statistician, pp. 169–178, 1992.

[18] T. Schlegl, T. Kröger, A. Gaschler, O. Khatib, and H. Zangl, "Virtual whiskers: Highly responsive robot collision avoidance," in Intelligent Robots and Systems (IROS), 2013 IEEE/RSJ International Conference on, Nov 2013, pp. 5373–5379.

[19] T. Schlegl, "Open environment capacitive sensing for safety applications," Ph.D. dissertation, Graz University of Technology, 2014.